Matter and Radiation at Extremes | RESEARCH ARTICLE | scitation.org/journal/mre

Ultrafast probing of plasma ion temperature in proton–boron fusion by nuclear resonance fluorescence emission spectroscopy

Cite as: Matter Radiat. Extremes 7, 035901 (2022); doi: 10.1063/5.0078961
Submitted: 16 November 2021 • Accepted: 27 February 2022 •
Published Online: 25 March 2022

T.-T. Qin,[1] W. Luo,[1,a)] H.-Y. Lan,[1] and W.-M. Wang[2,a)]

AFFILIATIONS

[1]School of Nuclear Science and Technology, University of South China, Hengyang 421001, China
[2]Beijing Key Laboratory of Opto-electronic Functional Materials and Micro-nano Devices and Department of Physics, Renmin University of China, Beijing 100872, China

[a)]**Authors to whom correspondence should be addressed:** wenluo-ok@163.com and weiminwang1@ruc.edu.cn

ABSTRACT

Aneutronic fusion reactions such as proton–boron fusion could efficiently produce clean energy with quite low neutron doses. However, as a consequence, conventional neutron spectral methods for diagnosing plasma ion temperature would no longer work. Therefore, finding a way to probe the ion temperature in aneutronic fusion plasmas is a crucial task. Here, we present a method to realize ultrafast *in situ* probing of ^{11}B ion temperature for proton–boron fusion by Doppler broadening of the nuclear resonance fluorescence (NRF) emission spectrum. The NRF emission is excited by a collimated, intense γ-ray beam generated from submicrometer wires irradiated by a recently available petawatt (PW) laser pulse, where the γ-ray beam generation is calculated by three-dimensional particle-in-cell simulation. When the laser power is higher than 1 PW, five NRF signatures of a ^{11}B plasma can be clearly identified with high-resolution γ-ray detectors, as shown by our Geant4 simulations. The correlation between the NRF peak width and ^{11}B ion temperature is discussed, and it is found that NRF emission spectroscopy should be sensitive to ^{11}B ion temperatures $T_i > 2.4$ keV. This probing method can also be extended to other neutron-free-fusion isotopes, such as ^{6}Li and ^{15}N.

I. INTRODUCTION

Inertial confinement fusion (ICF) and magnetic confinement fusion (MCF) research over the past 40 years has been focused on the reaction of deuterium (D) and tritium (T) nuclei under near-equilibrium conditions.[1–3] As the simplest binary nuclear reaction, the DT reaction is adopted because of its higher thermal reaction rate at relatively low temperatures (5–10 keV) compared with those of other light isotopes.[4] However, this reaction can generate high fluxes of high-energy neutrons, leading to a significant radiation hazard and the production of nuclear waste. Recent advances in laser technology,[5] laser–plasma interactions,[6] and laser-driven particle beams[7–10] provide great potential for the development of nuclear reactions with substantially less high-energy radiation.[11,12] For example, aneutronic fusion[13,14] is a promising reaction for clean fusion energy production. Most of the energy released during aneutronic fusion is carried by charged particles (e.g., α particles and protons), rather than neutrons. Aneutronic fuels that are often considered include D^{3}He, ^{3}He^{6}Li, ^{3}He^{3}He, p^6Li, p^7Li, p^{11}B, and p^{15}N.[15,16] In the case of p^{11}B, with the reaction $p + {}^{11}\mathrm{B} = 3\alpha + 8.7$ MeV, the released energy is mainly in the form of charged α particles rather than neutrons.[17] As a result, such a reaction would overcome the difficult issues of energy recovery and nuclear activation that occur with the high-energy neutrons produced in the classical DT reaction. Moreover, ^{11}B is easier to obtain and handle than tritium.

Plasma ion temperature is an important parameter in nuclear fusion with either DT fuel[18,19] or aneutronic fusion fuel,[20] as well as in other plasma-based applications such as experimental astrophysics.[21] A wide range of neutron diagnostics[22] have been developed and implemented at different ICF and MCF facilities worldwide because DT fusion yields a large number of neutrons and is suitable for neutron-based measurements. Neutron diagnostics have been providing an indispensable approach to understand the performance of ICF implosions. However, such measurements are passive and rely on emitted neutrons from the plasma, and therefore

they are not suitable for plasmas with low neutron yields (e.g., aneutronic fusion plasmas).

To overcome this limitation, *in situ* thermometry using nuclear resonance fluorescence (NRF)[23] has been proposed for ultrafast measurement of ion temperature in high-energy-density (HED) plasmas, particularly in aneutronic fusion research. This thermometry technique exploits the Doppler broadening of NRF emission lines. Because the broadening is sensitive to only the ion temperature and not the electron temperature, it could provide a clean and robust method to measure ion temperature in optically thick plasmas. Yu and Shen[24] investigated theoretically the probing of ion temperature dynamics in HED plasmas composed of ^{6}Li. They gave detection thresholds for ion temperature and plasma density, where a quasi-monoenergetic γ-ray source was employed and the detection of NRF emission lines was not considered.

In this article, we propose the use of Doppler broadening of NRF emission spectra, i.e., NRF emission spectroscopy, for *in situ* probing of ion temperature in proton–boron fusion plasmas (see the schematic in Fig. 1). In this scheme, a high flux γ-ray beam in an appropriate energy range is required to excite possible NRF processes inside the ^{11}B pellet and then to achieve sufficient probe precision. Hence, we take a collimated intense γ-ray beam generated from a solid wire irradiated by a recently available petawatt (PW) laser beam. Here, ^{11}B is chosen as a typical aneutronic fusion fuel,[25] and proton–boron fusion produces little high-energy radiation. For the ^{11}B nucleus, the resulting NRF emissions have relatively high energies, with considerable integrated cross sections.[26] The dependence of the laser power on the NRF yield is investigated, and the effect of ^{11}B ion temperature on the detectable NRF width is analyzed, with both the intrinsic Doppler broadening and the achievable energy resolution of state-of-the-art detectors being considered. The application of this scheme to other neutron-free-fusion isotopes,[27–29] such as ^{6}Li, ^{7}Li, and ^{15}N, is discussed. In addition, NRF emission spectroscopy can also be used for safeguard applications[30,31] and for nondestructive detection of special nuclear materials[32,48,49] and chemical compounds.[33]

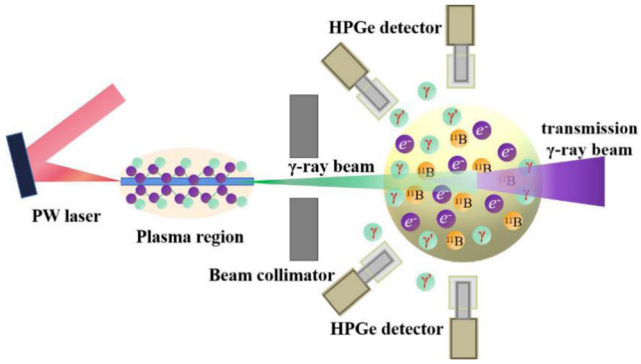

FIG. 1. Schematic of ultrafast probing of ion temperature in a hot ^{11}B plasma by Doppler broadening of NRF. An intense γ-ray beam can be efficiently generated from submicrometer wires irradiated by a recently available PW laser. After collimation, the γ-ray beam is fired into a ^{11}B pellet, which is located 11 cm downstream from the wire position and has a small radius of 2 mm, whereupon NRF interactions are excited. This is followed by emission of the characteristic photons. Owing to Doppler broadening, the NRF emission spectra contain information about ion temperature. To record these NRF signals efficiently, 24 high-purity germanium (HPGe) detectors are distributed in two concentric rings and are located at 90° and 135° with respect to the incident γ beam. The distance between the detectors and the pellet is 30 cm. For each detector, the germanium crystal used is 8.6 cm thick and has radius 4.2 cm. In our case, owing to the small size of the ^{11}B pellet, a large number of energetic γ rays will penetrate through the pellet, forming a transmitted γ-ray beam. For better visualization, the figure is not to scale.

II. THEORY

NRF processes involve resonant excitation of nuclear levels by photons and subsequent de-excitation. When the energy of an incoming photon E_0 is identical to the excitation energy of the target nucleus of interest, it can be effectively absorbed by that nucleus. In the first-order approximation, photons with energy E_0 in the laboratory system that are incident on a nucleus moving at the thermal velocity v in the beam propagation direction have a Doppler-shifted energy E' given by

$$E' = E_0\sqrt{\frac{1+v/c}{1-v/c}} = E_0\left(1+\frac{v}{c}\right), \tag{1}$$

where c is the speed of light in vacuum. Owing to the resonant absorption, the target nuclei are produced in excited states, which generally have extremely short lifetimes, and then rapidly de-excite by emitting γ photons isotropically. The energy of the γ rays emitted from a moving thermal nucleus is[24]

$$E \approx E_r + E_R' + E_r\frac{v}{c}. \tag{2}$$

Here, E_r is the energy of the photon emitted when the target nucleus decays to the ground state from the excited state without recoil and $E_R' \approx (2\cos\theta_1 - 1)E_R$, where θ_1 is the angle between the direction of emission of the photons and the direction of incidence of the γ-ray pulse and $E_R = E_r^2/(2M_ic^2)$ is the nuclear recoil energy associated with the photon emission.

The velocities of target nuclei in the direction of the incoming photon are distributed according to the one-dimensional Maxwell–Boltzmann distribution

$$w(v)dv = \sqrt{\frac{M_i}{2\pi k_B T_i}}\exp\left(-\frac{M_i v^2}{2k_B T_i}\right)dv, \tag{3}$$

where M_i is the mass of the target nucleus, T_i is the temperature of the target medium (i.e., the ion of interest), and k_B is Boltzmann's constant. Combining Eqs. (2) and (3), one obtains

$$w(E)dE = \frac{1}{\sqrt{2\pi}\Delta}\exp\left[-\left(\frac{E-E_R'-E_r}{\sqrt{2}\,\Delta}\right)^2\right]dE, \tag{4}$$

where Δ is the Doppler-broadened width (considering one standard deviation) and is defined as

$$\Delta = E_r\sqrt{\frac{k_B T_i}{M_i c^2}}. \tag{5}$$

This indicates that the Doppler broadening effect is caused primarily by the ion temperature.

When the ion temperature is higher than a few eV, which results in a Doppler-broadened width $\Delta > 100$ eV, the approximation $\Delta \gg \Gamma_r$ is satisfied and the Doppler-broadened cross section[34] can be expressed as

$$\sigma^{D}_{0,r,j}(E) = \pi^{3/2} g_r \left(\frac{\hbar c}{E_r}\right)^2 \frac{\Gamma_{0,r}\Gamma_{r,j}}{\sqrt{2}\Delta\Gamma_r} \exp\left[-\left(\frac{E - E'_R - E_r}{\sqrt{2}\,\Delta}\right)^2\right], \quad (6)$$

where $\hbar$ is the reduced Planck constant, $\Gamma_{0,r}$ is the partial width of the transition from the ground state (0) to the excited state r, $\Gamma_{r,j}$ is the partial width of the transition from the excited state r to a lower-energy state j, Γ_r is the total width of the excited state relative to its lifetime ($\Gamma_r \approx \hbar/\tau_r$), and $g_r = (2J_r + 1)/(2J_0 + 1)$ is the statistical factor, with J_r and J_0 being the total angular momenta of the nucleus in the resonant and ground states, respectively.

One can see that $\sigma^{D}_{0,r,j}(E)$ decreases dramatically owing to Doppler broadening. However, the integrated cross section does not change compared to the case without Doppler broadening. It can be seen from Fig. 2(a) that the Doppler-broadened cross section decreases with increasing ion temperature, but the Doppler-broadened width Δ varies inversely because of conservation of the integrated cross section. For ^{11}B at E_r = 5.020 MeV, the width Δ = 1.57 keV at T_i = 1 keV, and it increases to 4.96 keV at a higher temperature T_i = 10 keV. The Doppler-broadened cross section of ^{11}B is shown as a function of photon energy at resonance in Fig. 2(b). One can see that five Doppler-broadened cross sections at E_r = 2.125, 4.445, 5.020, 7.286, and 8.920 MeV are significant.

As mentioned above, an HPGe detector is used to detect emitted NRF photons in our study. The HPGe has an intrinsic resolution $\delta E_D = 2.36\sqrt{FIE'}$ at full width at half maximum (FWHM). Here, F = 0.13 is the Fano factor for germanium and I is the mean ionization energy (2.96 eV). In analogy with the error propagation formula, the width of the detected NRF peak (at FWHM) can be expressed as

$$\delta E = \sqrt{\delta E_D^2 + (2.355\Delta)^2}. \quad (7)$$

Thus, one could obtain a direct relation between the width δE and the ion temperature T_i by substituting Eq. (5) into Eq. (7). When T_i becomes high enough, the resulting 2.355Δ becomes comparable to or even higher than δE_D. For example, at T_i = 10 keV and E_r = 5.020 MeV, δE has a value of 12.13 keV. This is mainly affected by the ion temperature (the resulting 2.355Δ = 11.68 keV), rather than the intrinsic resolution of the detector (δE_D = 3.27 keV).

III. GENERATION OF COLLIMATED INTENSE GAMMA-RAY BEAM

Relativistic laser–plasma interaction can produce intense and high-energy γ-ray beams via betatron radiation,[35,36] inverse Compton scattering,[37,38] and other mechanisms. It has been shown that γ photons with energy exceeding a few MeV are very suitable for NRF excitations (see Fig. 2). To obtain such high-intensity γ-ray beams, we adopt a laser–wire scheme proposed in our previous work.[39] When a solid wire is irradiated by a PW laser beam, electron acceleration, guidance, and wiggling around the wire surface can be achieved simultaneously, which leads to the generation of directional high-energy, high-flux γ-ray beams. We use the three-dimensional particle-in-cell code KLAPS[40] to calculate the γ-ray source required for our probe. It includes photon generation via nonlinear Compton scattering and electron–positron pair creation via the multiphoton Breit–Wheeler process.[41] The simulation setup and parameters are the same as those presented in Ref. 39, namely, a PW laser beam with linear polarization, wavelength 800 nm, and duration 20 fs (FWHM) propagating along an aluminum wire 50 μm long and 0.6 μm wide.

We examine the spectral–angular distributions of γ-ray pulses under different laser peak powers. Figure 3 shows that with a currently available laser power P_0 ranging from 0.5 to 5 PW, the laser–wire scheme can robustly produce γ rays peaked at 1° (with respect to the laser axis). This is because the wiggling electrons are restricted around the wire surface by self-generated static electric and magnetic fields, which enables substantial emission of high-energy photons along the laser propagation direction. During laser–wire interaction, the electrons near the target surface are not always guided by the surface static fields and are mainly acted on by the laser fields, and the resulting photons also have larger divergent angles peaking around 12°. The cutoff energy of the generated photons increases with increasing laser power (see Fig. 3). It exceeds 100 MeV for a driven laser of 0.5 PW. In fact, the intensity of highly collimated γ rays within the energy range covering the NRF peaks is of great interest (see Fig. 2). For laser powers P_0 = 0.5, 1.0, 2.5, and 5.0 PW, the total photon numbers obtained within 4π solid angle are 3.71 × 10^{11}, 7.68 × 10^{11},

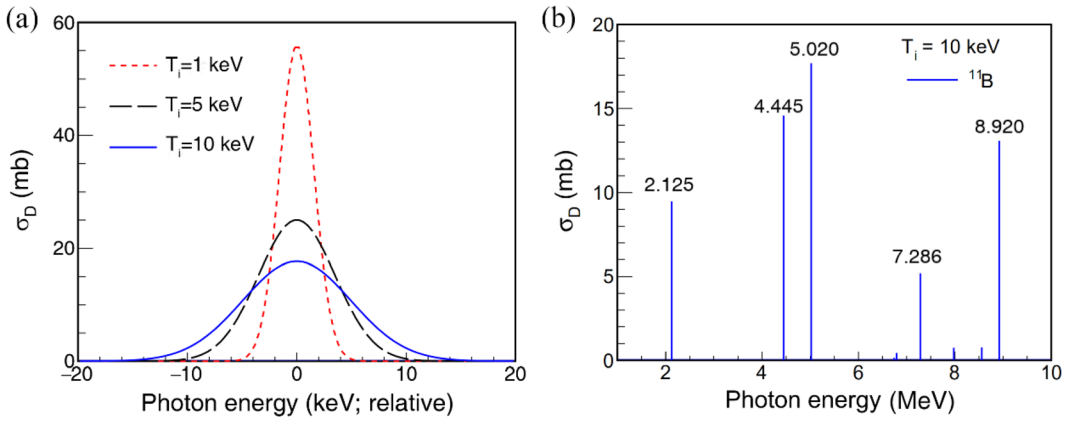

FIG. 2. (a) Dependence of Doppler-broadened cross section on ^{11}B ion temperature at E_r = 5.020 MeV. (b) Doppler-broadened cross section of ^{11}B as a function of photon energy.

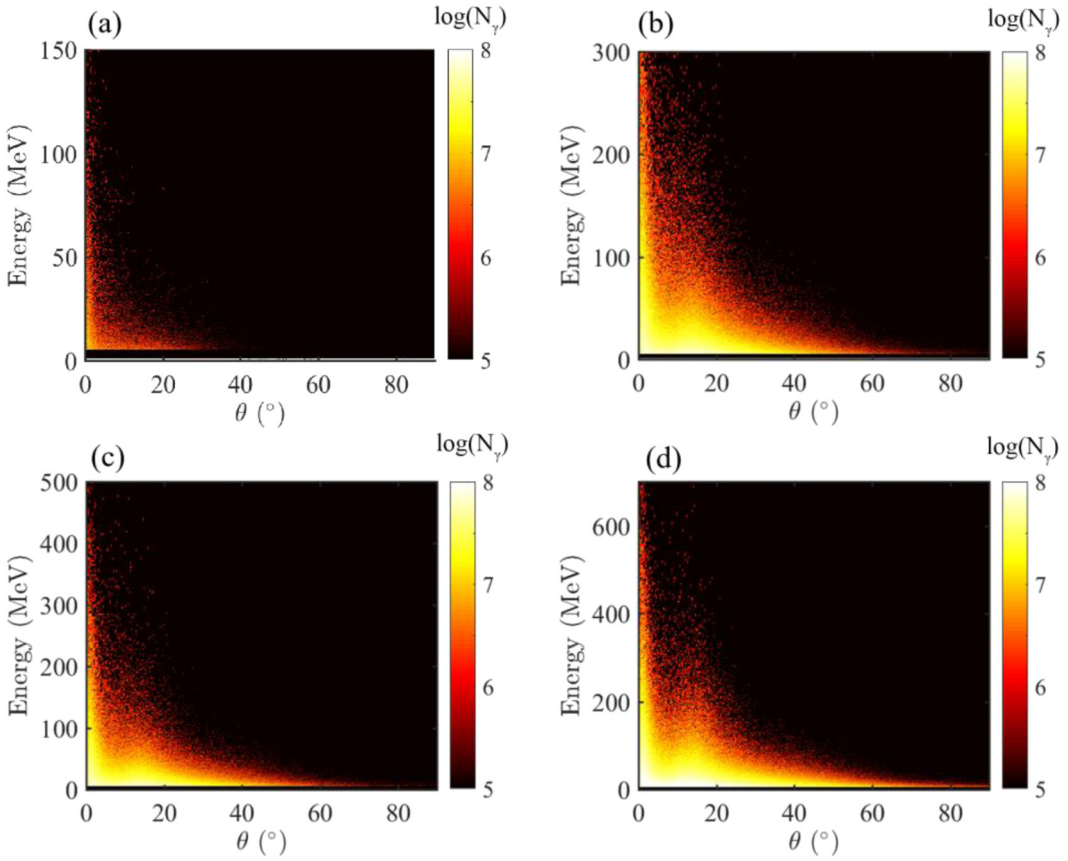

FIG. 3. Spectral–angular distribution of γ-ray pulses emitted from laser-illuminated wires under laser powers P_0 = 0.5 PW (a), 1.0 PW (b), 2.5 PW (c), and 5.0 PW (d).

2.36×10^{12}, and 5.02×10^{12}, respectively. The photon number and energy scale roughly with $P_0^{3/2}$ and P_0, respectively.[39]

Figure 3 also shows that a small proportion of the γ rays have a relatively large divergence angle. To avoid unnecessary irradiation of the pellet, proper collimation for such a γ-ray pulse is needed. For a collimation angle of 1°, the spectra of γ-ray beams injected onto the ^{11}B pellet are shown in Fig. 4. Accordingly, the numbers of photons are 1.74×10^{10}, 3.93×10^{10}, 1.06×10^{11}, and 1.85×10^{11} when $P_0 = 0.5$, 1.0, 2.5, and 5.0 PW, respectively. Note that the yields of photons after collimation decrease by one order of magnitude compared with those obtained before collimation. The tail of each spectrum can be approximated by an exponential temperature fit $N_\gamma = \exp(-E_\gamma/k_B T_\gamma)$ with an effective photon temperature T_γ, which is presented in Fig. 4. It can be seen that a collimated photon beam with energies within the NRF region of interest has a high spectral density approaching 10^6 photons/keV at P_0 = 2.5 PW.

IV. PROBING OF ^{11}B ION TEMPERATURE BY NRF

A. NRF signatures of ^{11}B plasmas

We have developed a new class, G4NRF, in the Geant4 toolkit[42–44] to model NRF interactions. Customizing the simulation to include the NRF process requires the NRF cross sections. In this study, the distributions of $\sigma^D_{0,r,j}(E)$ (see Fig. 2) are implemented into the G4NRF class. The transitions of ^{11}B ions in excited states to the ground state and to low-lying excited states are both taken into account. In the simulation setup, the effective ion temperature is set to $T_i = 10$ keV by default, to treat the pellet as a plasma. The ^{11}B ions have an isotropic velocity distribution with ion temperature T_i as described by Eq. (3). The collimated intense γ beams shown in Fig. 4 are used for irradiation. A detector array consisting of 24 HPGe detectors is used to record the emitted photons from the ^{11}B plasma with an areal density of 2.34 g/cm^2. A lead plate is installed at the front of each of HPGe detector to decrease the low-energy background and thus to increase the significance of NRF signals. In our case, the lead plate thickness is optimized to be 1 cm.

The photon number per unit energy (dE) and unit solid angle ($d\Omega$) is shown in Fig. 5(a). Four NRF signatures at higher energies (4.445, 5.020, 7.286, and 8.920 MeV) with relatively large $\sigma^D_{0,r,j}(E)$ (see Fig. 2) can clearly be seen in the green rings, since the photon energy is represented by the radius. Two single-escape (SE) peaks from signatures at 7.286 and 8.920 MeV and a double-escape (DE) peak from the one at 8.920 MeV can also be observed. Annihilation photons at 0.511 MeV are shown by the blue line. The NRF signature at 2.125 MeV is invisible because of the strong and continuous background from Compton scattering. As shown in Fig. 5(a), the NRF signatures and

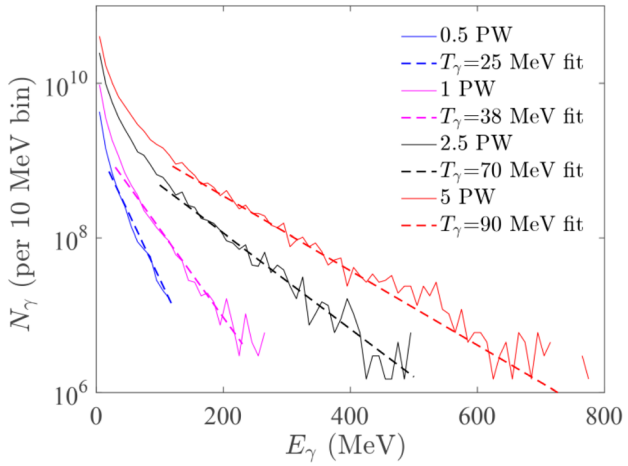

FIG. 4. Spectra of the γ-ray beams with collimation angle <1° at four different laser peak powers. The tails of these spectra are overlaid with exponential temperature fits, shown by broken lines.

their escape peaks are distributed in two sectors around $\theta = 90^\circ$ and 135°, as a result of the detector configuration shown in Fig. 1.

The NRF signatures can be more clearly observed in Fig. 5(b), which shows the sum of the NRF γ-ray spectra recorded by the 24 HPGe detectors. In contrast to Fig. 5(a), the NRF signature at 2.125 MeV can be distinguished from the continuous γ-ray background, besides other four NRF signatures and the positron annihilation peak at 0.511 MeV. The inset in Fig. 5(b) shows an enlarged view of the exemplary NRF signature at 5.020 MeV. NRF peaks can be reproduced well by Gaussian distributions and the NRF yields recorded can be obtained accordingly. For the NRF peak at 5.020 MeV, the simulated width $\delta E_{\rm sim} = 12.07$ keV, which is extracted from the fitting curve of Fig. 5(b), agrees with the theoretical value from Eq. (7). Since $\delta E_{\rm sim}$ provides accurate information on ion temperature, NRF emission spectroscopy combined with an intense γ-ray beam produced in relativistic laser–wire interactions can be used to probe the ion temperature in hot plasmas.

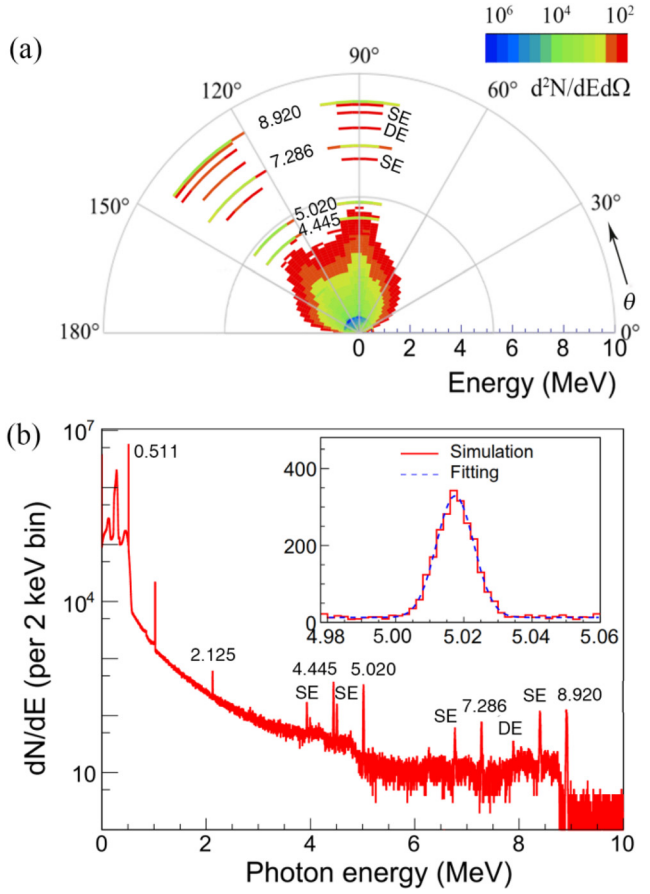

FIG. 5. Simulation results for a collimated intense γ-ray beam with effective temperature $T_\gamma = 70$ MeV at a laser power of 2.5 PW. (a) γ-ray intensity recorded by 24 HPGe detectors as a function of observing angle θ and energy (which is represented by the radius in the polar figure). (b) γ-ray spectrum showing five NRF signatures and a few escape peaks. The inset shows an enlarged view of one NRF signature at 5.020 MeV. The dashed line is a fitting curve of a Gaussian distribution.

B. Effect of ion temperature

To predict the lower threshold of (^{11}B) ion temperature that can be probed by NRF emission spectroscopy, we investigate the effect of ion temperature on the width of the simulated NRF peak, as shown in Fig. 6(a). The width $\delta E_{\rm sim}$ increases with increasing ion temperature T_i. The resulting spectral broadening effect becomes significant for $T_i > 1$ keV at $E_r = 5.020$ MeV. The results for $\delta E_{\rm sim}$, δE, 2.355 Δ, and δE_D as functions of T_i are shown in Fig. 6(b), in which the detection threshold for T_i can be observed more clearly. The relative deviations between $\delta E_{\rm sim}$ and δE are smaller than 5% when 0.1 keV < T_i < 10 keV, indicating that the simulations are in good agreement with the theoretical results. At relatively high ion temperatures for ion plasmas, the variation of $\delta E_{\rm sim}$ deviates gradually from that of δE_D, which is independent of T_i. Generally, when the value of $\delta E_{\rm sim}$ is twice the intrinsic width of the detector (δE_D), one can readily see the effect of Doppler broadening on the peak width and then extract information on the ion temperature. As T_i increases to 2.4 keV, $2.355\Delta = 5.72$ keV, which gives $\delta E_{\rm sim} = 6.54$ keV. Both 2.355Δ and $\delta E_{\rm sim}$ are clearly higher than δE_D, indicating that the Doppler broadening effect will play a key role in $\delta E_{\rm sim}$ when T_i is higher than 2.4 keV. We conclude that in the scenario of proton–boron fusion, our proposed method is able to effectively probe ion temperatures $T_i > 2.4$ keV.

C. Effect of laser peak power

A certain number of NRF emission photons, which pile up into a NRF peak, is a prerequisite for analysis of the ion temperature by Doppler broadening of the NRF photon spectrum. The NRF yield is correlated linearly with the product of the NRF cross section and the incident photon intensity. The impact of laser peak power on NRF yield is shown in Fig. 7(a). The NRF yield increases rapidly with increasing P_0. For $P_0 \geq 1.0$ PW, such a yield can result in the clear NRF peaks observed by the HPGe detector array. This is mainly attributable to an increased intensity of γ photons within the NRF region of interest. When P_0 is fixed, the NRF yields for the five NRF γ lines are

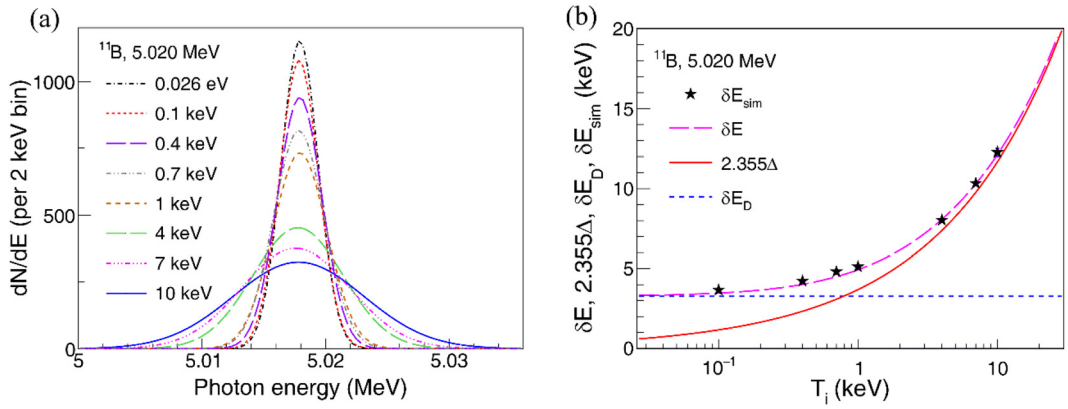

FIG. 6. (a) Fitting curves of NRF peaks at 5.020 MeV. A collimated intense γ-ray beam with temperature T_γ = 70 MeV at laser power 2.5 PW is used for the simulation. (b) Values of δE_{sim}, δE, 2.355Δ, and δE_D at 5.020 MeV as functions of ion temperature T_i.

affected primarily by the NRF cross section, owing to the very close photon intensity (see Fig. 4). This is the reason why the simulated NRF yields at E_r = 4.445 and 5.020 MeV are much higher than those obtained at 2.125, 7.286, and 8.920 MeV.

It is interesting to discuss the lower threshold areal density of ^{11}B plasma required for the formation of an NRF peak. Supposing the NRF peak to be composed simply of 100 NRF photons piled up in the detector, one can readily obtain the dependence of the required areal density on P_0. Figure 7(b) presents the relation between the areal density and P_0. The required areal density decreases with increasing laser power. At P_0 = 5 PW, the areal density required for probing the ^{11}B ion temperature approaches 0.1 g/cm^2. In addition, the areal densities required at the two NRF lines of 4.445 and 5.020 MeV are clearly lower than those at 2.125, 7.286, and 8.920 MeV. The detected NRF yields are still dependent on the areal density of the ^{11}B plasma. Additional simulations show that the NRF yields for the five NRF lines mentioned above first increase with areal density, and then become saturated at an areal density of ~30 g/cm^2, since the γ-ray beam is attenuated mainly by the atomic absorption effect. It is expected that our proposed method will be valid when the areal density of the ^{11}B plasma is higher than 30 g/cm^2.

D. Possible application to other aneutronic fusion isotopes

Besides the ^{11}B isotope, there are other isotope materials such as ^{6}Li, ^{7}Li, and ^{15}N that are suitable for aneutronic fusion studies.[27–29] We shall now discuss the feasibility of performing ion temperature diagnostics for these fusion plasmas using NRF emission spectroscopy. Under the premise that $\delta E_{sim} \geq 2\delta E_D$, ion temperature thresholds T_i^{th} are estimated for these neutron-free-fusion isotopes. The results are summarized in Table I. It can be seen that for ^{6}Li, ^{11}B, and ^{15}N, the ion temperature thresholds are about 2 keV, which is obviously lower than the normal temperature required for fusion ignition. Note that since ^{7}Li has insignificant values for both I_σ and E_r (see Table I), it requires a much higher photon density in the energy region of nuclear excitation. The ion temperature threshold of ^{7}Li is almost one order of magnitude higher than that for the other isotope materials.

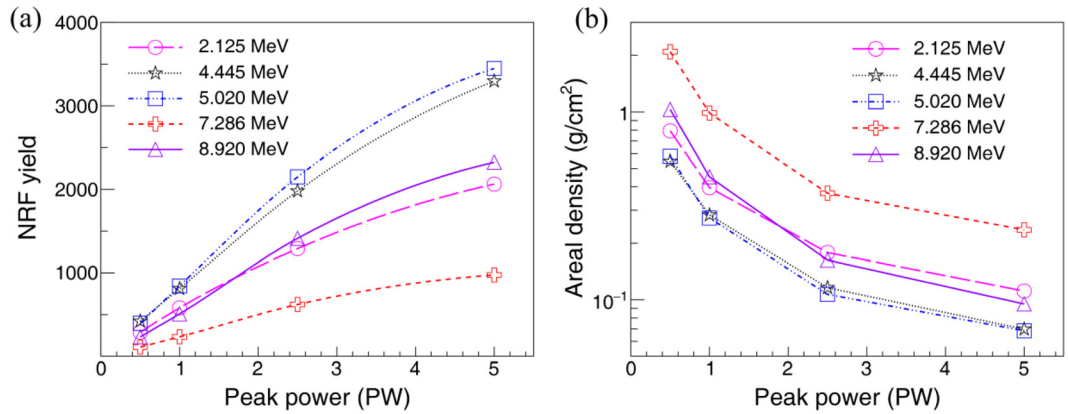

FIG. 7. Dependence of the detected NRF yield (a) and areal density (b) on laser peak power with ^{11}B ions at resonance energies of 2.125, 4.445, 5.020, 7.286, and 8.920 MeV. The NRF yield is fixed at 100 for calculating the required areal density in (b).

TABLE I. Integrated NRF cross sections I_σ for principal transitions $0 \rightarrow r \rightarrow 0$ in ^{6,7}Li, ^{11}B, and ^{15}N at their characteristic energies E_r and the estimated thresholds to probe ion temperature under the premise that $\delta E_{\rm sim} \geq 2\delta E_D$.

Isotope	J_0^π	J_r^π	E_r (MeV)	I_σ (b eV)	δE_D (keV)	$\delta E_{\rm sim}$ (keV)	$T_i^{\rm th}$ (keV)
^{6}Li	1^+	0^+	3.563	830	2.75	5.50	1.9
^{7}Li	$3/2^-$	$1/2^-$	0.478	53	1.00	2.00	16.0
^{11}B	$3/2^-$	$3/2^-$	5.020	220	3.27	6.54	2.4
^{15}N	$1/2^-$	$3/2^-$	6.324	600	3.67	7.34	2.6

Areal density thresholds are further evaluated for these isotope materials. The results are shown in Fig. 8, where the resonance energies are 3.563, 0.478, 5.020, and 6.324 MeV for ^{6}Li, ^{7}Li, ^{11}B, and ^{15}N, respectively. It is found that ^{6}Li has an areal density as low as 0.04 g/cm^2, which is ~5 times smaller than those of ^{11}B and ^{15}N owing to a large I_σ (see Table I). Such an areal density is one order of magnitude lower than that found in previous studies,[24] because the wire-guided PW laser can generate a highly directed photon beam with high spectral density of 10^5–10^6 photons/keV at E_r = 3.563 MeV (see Fig. 4). Note that ^{7}Li would not be a good candidate, owing to its relatively small resonant energy. Temperature diagnosis of ^{7}Li would confront a stronger background than in the cases of the other isotope materials.

V. DISCUSSION

In the simulations, a ^{11}B plasma with uniform density and temperature was employed by default. For a plasma that is non-uniform in density and temperature, for example, when the plasma density ramps-up and ramps-down on both ends (but the areal density remains the same on average), the simulated NRF yield varies insignificantly (within statistical uncertainty) compared with the uniform-density case. To probe the ion temperature successfully, the backgrounds from target irradiation need to be suppressed in an effective way. This is because strong backgrounds may hit the detector simultaneously with the NRF signals, leading to a pile-up effect on the HPGe detector, and may also broaden the NRF peak width to some extent. Owing to the complexity of the pile-up effect, we did not consider it in the present Geant4 simulations. Three practicable approaches are suggested to alleviate event pile-up: (1) installing a lead plate in front of each detector, which can filter out a large number of background photons at relatively low energies; (2) increasing the distance between the detectors and the ^{11}B pellet, which has the advantage of increasing the available space and thus enabling the use of more detectors for spectral accumulation; and (3) optimizing the energy spread of the γ-ray beam to achieve a good match with the NRF energy level of interest.

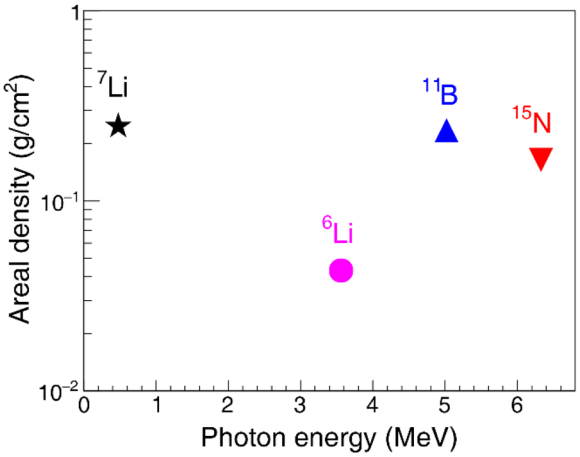

FIG. 8. Threshold areal density required for four aneutronic fusion materials. The resonance energy E_r is selected to be 3.563, 0.478, 5.020, and 6.324 MeV for ^{6}Li, ^{7}Li, ^{11}B, and ^{15}N, respectively. A collimated intense γ-ray beam with temperature T_γ = 38 MeV at 1.0 PW laser power is used.

In addition, studies have shown that pile-up pulses can be effectively disentangled using a digital data acquisition system with appropriate algorithms, and then most of the information carried by the overlapping pulses can be precisely recorded.[45] For detection of instantaneous photons, an advanced gamma tracking array,[46] which contains more than one hundred 36-fold segmented HPGe crystals, has been developed. A multidetector array called ELIADE[47] has been constructed to measure NRF at the Extreme Light Infrastructure–Nuclear Physics in Romania.

Considering that the confinement time in an ICF implosion is of the order of picoseconds, the challenge is how to probe ion temperature using a single laser shot. The feasibility of doing this depends on the event pile-up and its disentanglement and on whether the number of detectors used for recording the NRF signal is sufficient or not. More effort is needed to resolve this issue.

VI. CONCLUSIONS

The method of NRF emission spectroscopy discussed here allows ultrafast *in situ* probing of ion temperature in aneutronic fusion plasmas. To efficiently excite the NRF process in such plasmas, a collimated intense γ-ray beam, which can be generated in the interaction of a PW laser beam with a submicrometer wire, is adopted. The NRF yield recorded by an HPGe detector increases rapidly with increasing laser power. In the case of ^{11}B ion plasmas, five NRF signatures can be identified, since the laser-generated photon beams have sufficiently high spectral density within the NRF region of interest. The Doppler broadening effect resulting from the ion temperature is then observed, and this simulated result shows good agreement with the theoretical prediction. NRF emission spectroscopy has the potential to diagnose ^{11}B plasmas with a lower threshold areal density of the order of 0.1 g/cm^2 and with an ion temperature exceeding 2.4 keV.

Further investigations have shown that this method can be extended to other aneutronic fusion scenarios, including those involving the ^{6}Li and ^{15}N isotopes. This suggests that NRF emission

spectroscopy is an appropriate method for probing plasma ion temperatures for HED physics research, especially with aneutronic fusion plasmas. The method should also be applicable in safeguards and in nondestructive detection of special nuclear materials and chemical compounds, etc.

ACKNOWLEDGMENTS

This work was supported by the National Natural Science Foundation of China (Grant Nos. 11675075 and 11775302), the Youth Talent Project of Hunan Province, China (Grant No. 2018RS3096), the Independent Research Project of the Key Laboratory of Plasma Physics, CAEP (Grant No. JCKYS2021212009), the Strategic Priority Research Program of the Chinese Academy of Sciences (Grant No. XDA25050300), the National Key R&D Program of China (Grant No. 2018YFA0404801), the Research Project of NUDT (Grant No. ZK18-02-02), and the Fundamental Research Funds for the Central Universities, the Research Funds of Renmin University of China (Grant No. 20XNLG01).

AUTHOR DECLARATIONS

Conflict of Interest

The authors have no conflicts to disclose.

DATA AVAILABILITY

The data that support the findings of this study are available from the corresponding author upon reasonable request.

REFERENCES

[1]J. Nuckolls, L. Wood, A. Thiessen, and G. Zimmerman, "Laser compression of matter to super-high densities: Thermonuclear (CTR) applications," Nature **239**, 139–142 (1972).

[2]J. Lindl, "Development of the indirect-drive approach to inertial confinement fusion and the target physics basis for ignition and gain," Phys. Plasmas **2**, 3933–4024 (1995).

[3]J. Ongena, R. Koch, R. Wolf, and H. Zohm, "Magnetic-confinement fusion," Nat. Phys. **12**, 398–410 (2016).

[4]S. Atzeni and J. Meyer-Ter-Vehn, *The Physics of Inertial Fusion* (Oxford Science Publication, 2004).

[5]D. Strickland and G. Mourou, "Compression of amplified chirped optical pulses," Opt. Commun. **55**, 447–449 (1985).

[6]D. Pesme and C. Labaune, in *La Fusion Thermonucleaire Inertielle par Laser*, edited by R. Dautray and J. P. Watteau (Eyrolles, 1993), Vol. 1.

[7]A. P. Fews, P. A. Norreys, F. N. Beg, A. R. Bell, A. E. Dangor, C. N. Danson, P. Lee, and S. J. Rose, "Plasma ion emission from high intensity picosecond laser pulse interactions with solid targets," Phys. Rev. Lett. **73**, 1801–1804 (1994).

[8]A. Maksimchuk, S. Gu, K. Flippo, D. Umstadter, and V. Y. Bychenkov, "Forward ion acceleration in thin films driven by a high-intensity laser," Phys. Rev. Lett. **84**, 4108–4111 (2000).

[9]R. A. Snavely, M. H. Key, S. P. Hatchett, T. E. Cowan, M. Roth, T. W. Phillips, M. A. Stoyer, E. A. Henry, T. C. Sangster, M. S. Singh, S. C. Wilks, A. MacKinnon, A. Offenberger, D. M. Pennington, K. Yasuike, A. B. Langdon, B. F. Lasinski, J. Johnson, M. D. Perry, and E. M. Campbell, "Intense high-energy proton beams from petawatt-laser irradiation of solids," Phys. Rev. Lett. **85**, 2945–2948 (2000).

[10]J. Fuchs, P. Antici, E. d'Humières, E. Lefebvre, M. Borghesi, E. Brambrink, C. A. Cecchetti, M. Kaluza, V. Malka, M. Manclossi, S. Meyroneinc, P. Mora, J. Schreiber, T. Toncian, H. Pépin, and P. Audebert, "Laser-driven proton scaling laws and new paths towards energy increase," Nat. Phys. **2**, 48–54 (2006).

[11]V. T. Voronchev and V. I. Kukulin, "Nuclear-physics aspects of controlled thermonuclear fusion: Analysis of promising fuels and gamma-ray diagnostics of hot plasma," Phys. At. Nucl. **63**, 2051–2066 (2000).

[12]W. M. Nevins, "A review of confinement requirements for advanced fuels," J. Fusion Energy **17**, 25–32 (1998).

[13]D. Giulietti, P. Andreoli, D. Batani *et al.*, "Laser-plasma energetic particle production for aneutronic nuclear fusion experiments," Nucl. Instrum. Methods Phys. Res., Sect. B **402**, 373–375 (2017).

[14]C. Baccou, S. Depierreux, V. Yahia *et al.*, "New scheme to produce aneutronic fusion reactions by laser-accelerated ions," Laser Part. Beams **33**, 117–122 (2015).

[15]B. Nayak, "Reactivities of neutronic and aneutronic fusion fuels," Ann. Nucl. Energy **60**, 73–77 (2013).

[16]J. Gruenwald, "Proposal for a novel type of small scale aneutronic fusion reactor," Plasma Phys. Controlled Fusion **59**, 025011 (2016).

[17]H. W. Becker, C. Rolfs, and H. P. Trautvetter, "Low-energy cross sections for ^{11}B(p,3α)," Z. Phys. A: At. Nucl. **327**, 341–355 (1987).

[18]R. C. Kirkpatrick and J. A. Wheeler, "The physics of DT ignition in small fusion targets," Nucl. Fusion **21**, 389–401 (1981).

[19]N. Rostoker, M. W. Binderbauer, and H. J. Monkhorst, "Colliding beam fusion reactor," Science **278**, 1419–1422 (1997).

[20]H. Hora, G. H. Miley, S. Eliezer, and N. Nissim, "Pressure of picosecond CPA laser pulses substitute ultrahigh thermal pressures to ignite fusion," High Energy Density Phys. **35**, 100739 (2020).

[21]D. T. Casey, D. B. Sayre, C. R. Brune, V. A. Smalyuk, C. R. Weber, R. E. Tipton, J. E. Pino, G. P. Grim, B. A. Remington, D. Dearborn, L. R. Benedetti, J. A. Frenje, M. Gatu-Johnson, R. Hatarik, N. Izumi, J. M. McNaney, T. Ma, G. A. Kyrala, S. MacLaren, J. Salmonson, S. F. Khan, A. Pak, L. B. Hopkins, S. LePape, B. K. Spears, N. B. Meezan, L. Divol, C. B. Yeamans, J. A. Caggiano, D. P. McNabb, D. M. Holunga, M. Chiarappa-Zucca, T. R. Kohut, and T. G. Parham, "Thermonuclear reactions probed at stellar-core conditions with laser-based inertial-confinement fusion," Nat. Phys. **13**, 1227–1231 (2017).

[22]V. Y. Glebov, T. C. Sangster, C. Stoeckl, J. P. Knauer, W. Theobald, K. L. Marshall, M. J. Shoup, T. Buczek, M. Cruz, T. Duffy, M. Romanofsky, M. Fox, A. Pruyne, M. J. Moran, R. A. Lerche, J. McNaney, J. D. Kilkenny, M. J. Eckart, D. Schneider, D. Munro, W. Stoeffl, R. Zacharias, J. J. Haslam, T. Clancy, M. Yeoman, D. Warwas, C. J. Horsfield, J.-L. Bourgade, O. Landoas, L. Disdier, G. A. Chandler, and R. J. Leeper, "The National Ignition Facility neutron time-of-flight system and its initial performance (invited)," Rev. Sci. Instrum. **81**, 10D325 (2010).

[23]C. T. Angell, "Enabling *in situ* thermometry using transmission nuclear resonance fluorescence," Nucl. Instrum. Methods Phys. Res., Sect. B **368**, 9–14 (2016).

[24]Y. Yu and B. Shen, "Ultrafast measurements of ion temperature in high-energy-density plasmas by nuclear resonance fluorescence," Phys. Plasmas **26**, 062708 (2019).

[25]H. Hora, G. Korn, S. Eliezer, N. Nissim, P. Lalousis, L. Giuffrida, D. Margarone, A. Picciotto, G. H. Miley, S. Moustaizis, J.-M. Martinez-Val, C. P. J. Barty, and G. J. Kirchhoff, "Avalanche boron fusion by laser picosecond block ignition with magnetic trapping for clean and economic reactor," High Power Laser Sci. Eng. **4**, e35 (2016).

[26]P. Mohr, T. Hartmann, K. Vogt, S. Volz, and A. Zilges, "Electric dipole strength below the giant dipole resonance," AIP Conf. Proc. **610**, 870–874 (2002).

[27]X. Z. Li, Z. M. Dong, and C. L. Liang, "Studies on p+^{6}Li fusion reaction using 3-parameter model," J. Fusion Energy **31**, 432–436 (2012).

[28]M. Ghoranneviss, A. Salar Elahi, H. Hora, G. H. Miley, B. Malekynia, and Z. Abdollahi, "Laser fusion energy from p-^{7}Li with minimized radioactivity," Laser Part. Beams **30**, 459–463 (2012).

[29]D. G. Kovar, D. F. Geesaman, T. H. Braid, Y. Eisen, W. Henning, T. R. Ophel, M. Paul, K. E. Rehm, S. J. Sanders, P. Sperr, J. P. Schiffer, S. L. Tabor, S. Vigdor, B. Zeidman, and F. W. Prosser, "Systematics of carbon- and oxygen-induced fusion on nuclei with 12 ≤ A ≤ 19," Phys. Rev. C **20**(4), 1305 (1979).

[30]R. S. Kemp, A. Danagoulian, R. R. Macdonald, and J. R. Vavrek, "Physical cryptographic verification of nuclear warheads," Proc. Natl. Acad. Sci. U. S. A. **113**(31), 8618–8623 (2016).

[31]J. R. Vavrek, B. S. Henderson, and A. Danagoulian, "Experimental demonstration of an isotope-sensitive warhead verification technique using nuclear resonance fluorescence," Proc. Natl. Acad. Sci. U. S. A. **115**(17), 4363–4368 (2018).

[32]J. Pruet, D. P. McNabb, C. A. Hagmann, F. V. Hartemann, and C. P. J. Barty, "Detecting clandestine material with nuclear resonance fluorescence," J. Appl. Phys. **99**(12), 123102 (2006).
[33]T. Hayakawa, H. Ohgaki, T. Shizuma, R. Hajima, N. Kikuzawa, E. Minehara, T. Kii, and H. Toyokawa, "Nondestructive detection of hidden chemical compounds with laser Compton-scattering gamma rays," Rev. Sci. Instrum. **80**(4), 045110 (2009).
[34]F. R. Metzger, "Resonance fluorescence in nuclei," Prog. Nucl. Phys. **7**, 54 (1959).
[35]A. Rousse, K. T. Phuoc, R. Shah, A. Pukhov, E. Lefebvre, V. Malka, S. Kiselev, F. Burgy, J.-P. Rousseau, D. Umstadter, and D. Hulin, "Production of a keV x-ray beam from synchrotron radiation in relativistic laser-plasma interaction," Phys. Rev. Lett. **93**(13), 135005 (2004).
[36]K. Németh, B. Shen, Y. Li, H. Shang, R. Crowell, K. C. Harkay, and J. R. Cary, "Laser-driven coherent betatron oscillation in a laser-wakefield cavity," Phys. Rev. Lett. **100**(9), 095002 (2008).
[37]K. Ta Phuoc, S. Corde, C. Thaury, V. Malka, A. Tafzi, J. P. Goddet, R. C. Shah, S. Sebban, and A. Rousse, "All-optical Compton gamma-ray source," Nat. Photonics **6**(5), 308–311 (2012).
[38]C. Liu, G. Golovin, S. Chen, J. Zhang, B. Zhao, D. Haden, S. Banerjee, J. Silano, H. Karwowski, and D. Umstadter, "Generation of 9 MeV γ-rays by all-laser-driven Compton scattering with second-harmonic laser light," Opt. Lett. **39**(14), 4132–4135 (2014).
[39]W.-M. Wang, Z.-M. Sheng, P. Gibbon, L.-M. Chen, Y.-T. Li, and J. Zhang, "Collimated ultrabright gamma rays from electron wiggling along a petawatt laser-irradiated wire in the QED regime," Proc. Natl. Acad. Sci. U. S. A. **115**(40), 9911–9916 (2018).
[40]W. M. Wang, P. Gibbon, Z. M. Sheng, and Y. T. Li, "Integrated simulation approach for laser-driven fast ignition," Phys. Rev. E **91**, 013101 (2015).
[41]W. M. Wang, P. Gibbon, Z. M. Sheng, Y. T. Li, and J. Zhang, "Laser opacity in underdense preplasma of solid targets due to quantum electrodynamics effects," Phys. Rev. E **96**, 013201 (2017).
[42]S. Agostinelli, J. Allison, K. Amako, J. Apostolakis, H. Araujo, P. Arce, M. Asai, D. Axen, S. Banerjee, G. Barrand, F. Behner, L. Bellagamba, J. Boudreau, L. Broglia, A. Brunengo, H. Burkhardt, S. Chauvie, J. Chuma, R. Chytracek, G. Cooperman *et al.*, "GEANT4—A simulation toolkit," Nucl. Instrum. Methods Phys. Res., Sect. A **506**(3), 250–303 (2003).
[43]W. Luo, H.-y. Lan, Y. Xu, and D. L. Balabanski, "Implementation of the n-body Monte-Carlo event generator into the Geant4 toolkit for photonuclear studies," Nucl. Instrum. Methods Phys. Res., Sect. A **849**, 49–54 (2017).
[44]H. Y. Lan, S. Tan, X. D. Huang, S. Q. Zhao, J. L. Zhou, Z. C. Zhu, Y. Xu, D. L. Balabanski, and W. Luo, "Nuclear resonance fluorescence drug inspection," Sci. Rep. **11**(1), 1306 (2021).
[45]D. W. Luo, H. Y. Wu, Z. H. Li, C. Xu, H. Hua, X. Q. Li, X. Wang, S. Q. Zhang, Z. Q. Chen, C. G. Wu, Y. Jin, and J. Lin, "Performance of digital data acquisition system in gamma-ray spectroscopy," Nucl. Sci. Tech. **32**(8), 79 (2021).
[46]S. Akkoyun, A. Algora, B. Alikhani, F. Ameil, G. de Angelis, L. Arnold, A. Astier, A. Ataç, Y. Aubert, C. Aufranc, A. Austin, S. Aydin, F. Azaiez, S. Badoer, D. L. Balabanski, D. Barrientos, G. Baulieu, R. Baumann, D. Bazzacco, F. A. Beck, T. Beck, P. Bednarczyk, M. Bellato, M. A. Bentley, G. Benzoni, R. Berthier, L. Berti, R. Beunard, G. Lo Bianco, B. Birkenbach, P. G. Bizzeti, A. M. Bizzeti-Sona, F. Le Blanc, J. M. Blasco, N. Blasi, D. Bloor, C. Boiano, M. Borsato, D. Bortolato, A. J. Boston, H. C. Boston, P. Bourgault *et al.*, "AGATA—Advanced gamma tracking array," Nucl. Instrum. Methods Phys. Res., Sect. A **668**, 26–58 (2012).
[47]C. A. Ur, A. Zilges, N. Pietralla, J. Beller, B. Boisdeffre, M. O. Cernaianu, V. Derya, B. Loher, C. Matei, G. Pascovici, C. Petcu, C. Romig, D. Savran, G. Suliman, E. Udup, and V. Werner, "Nuclear resonance fluorescence experiments at ELI-NP," Rom. Rep. Phys. **68**, S483–S538 (2016).
[48]H.-Y. Lan, T. Song, Z.-H. Luo, J.-L. Zhou, Z.-C. Zhu, and W. Luo, "Isotope-Sensitive Imaging of Special Nuclear Materials Using Computer Tomography Based on Scattering Nuclear Resonance Fluorescence," Phys. Rev. Applied **16**(5), 054048 (2021).
[49]H.-Y. Lan, T. Song, J.-L. Zhang, J.-L. Zhou, and W. Luo, "Rapid interrogation of special nuclear materials by combining scattering and transmission nuclear resonance fluorescence spectroscopy," Nucl. Sci. Tech. **32**(8), 84 (2021).